1D-VAR Retrieval of Temperature and Humidity Profiles From a Ground-Based Microwave Radiometer

Tim J. Hewison, *Member, IEEE*

Abstract—A variational method to retrieve profiles of temperature, humidity, and cloud is described, which combines observations from a 12-channel microwave radiometer, an infrared radiometer, and surface sensors with background from short-range numerical weather prediction (NWP) forecasts in an optimal way, accounting for their error characteristics. An analysis is presented of the error budget of the background and observations, including radiometric, modeling, and representativeness errors. Observation errors of some moisture channels are found to be dominated by representativeness, due to their sensitivity to atmospheric variability on smaller scales than the NWP model grid, whereas channels providing information on temperature in the lowest 1 km are dominated by instrument noise. Profiles of temperature and a novel total water control variable are retrieved from synthetic data using Newtonian iteration. An error analysis shows that these are expected to improve mesoscale NWP, retrieving temperature and humidity profiles up to 4 km with uncertainties of < 1 K and $< 40\%$ and 2.8 and 1.8 degrees of freedom for signal, respectively, albeit with poor vertical resolution. A cloud classification scheme is introduced to address convergence problems and better constrain the retrievals. This Bayesian retrieval method can be extended to incorporate observations from other instruments to form a basis for future *integrated profiling systems*.

Index Terms—Atmospheric measurements, microwave radiometry, remote sensing, variational methods.

I. INTRODUCTION

NUMERICAL weather prediction (NWP) and *nowcasting* applications have a requirement for observations of temperature and humidity profiles of increasing accuracy, frequency, and resolution. It is anticipated that these requirements may be addressed by integrating observations from different ground-based remote sensing instruments, including a microwave radiometer, to supplement the radiosonde network and to complement satellite data over land. These *integrated profiling systems* offer the potential to provide information on vertical profiles of temperature, humidity, and clouds at a high temporal resolution, which could be assimilated into the next generation of convective-scale NWP models. This paper demonstrates a 1-D variational (1D-VAR) retrieval method that can be used to combine observations from multiple instruments with background information from an NWP model to retrieve profiles of temperature and total water. The performance of these retrievals can be compared with user requirements.

The retrieval of temperature and humidity profiles from passive ground-based sensors is an *ill-posed* problem because there are an infinite number of atmospheric states that can produce a given observation vector within its uncertainty. This can be resolved by the addition of *background* data, for example, in the form of a short-range forecast from an NWP model. Variational retrievals provide an *optimal* method of combining observations with a background, which accounts for the assumed error characteristics of both. For this reason, they are often referred to as *optimal estimation* retrievals. The 1D-VAR retrievals that are presented here are similar to the *integrated profiling technique* [1], but they take their background from an NWP model instead of radiosondes and use different control variables to concentrate on retrieving temperature and humidity.

The 1D-VAR retrieval is performed by adjusting the atmospheric state vector $\mathbf{x}$ from the background state $\mathbf{x^b}$ to minimize a cost function of the following form [2]:

$$J(\mathbf{x}) = [\mathbf{x} - \mathbf{x^b}]^T \mathbf{B}^{-1} [\mathbf{x} - \mathbf{x^b}] + [\mathbf{y} - H(\mathbf{x})]^T \mathbf{R}^{-1} [\mathbf{y} - H(\mathbf{x})] \tag{1}$$

where $\mathbf{B}$ and $\mathbf{R}$ are the error covariance matrices of the background $\mathbf{x^b}$ and observation vector $\mathbf{y}$, respectively; $H(\mathbf{x})$ is the forward model operator; and ^{T} and $^{-1}$ are the matrix transpose and inverse, respectively, using standard notation [3].

II. BACKGROUND DATA AND STATE VECTOR

The mesoscale version of the Met Office Unified Model is used to provide background data for the retrievals in the form of profiles of temperature, humidity, and liquid water. The model grid points are interpolated to the position of the observations. This model is initiated every 6 h, including data from radiosonde stations. A short-range forecast ($T + 3$ h to $T + 9$ h) is used for the background, as would be available to operational assimilation schemes, and is independent of any radiosondes that are launched at observation time, which may be used to validate the retrievals.

The state vector $\mathbf{x}$ that is used in the retrievals is defined as the temperature and total water at the lowest 28 model levels. These extend up to 14 km but are concentrated near the surface, where most of the radiometer's information is.

In this paper, the humidity components of the state vector are defined as the natural log of total water, i.e., $\ln q_t$ (q is the

specific humidity). This control variable is a modified version of that suggested in [4], with a smooth transfer function between water vapor for $q_t/q_{sat} < 90\%$ and liquid water for $q_t/q_{sat} > 110\%$ (where q_{sat} is q at saturation) [5]. The condensed part of the total water is further partitioned between liquid and ice fractions as a linear function of temperature, producing pure ice at $-40\ ^\circ$C. The ice is ignored in the microwave forward model but absorbs like liquid in the infrared. The choice of total water has the advantages of reducing the dimension of the state vector, enforcing an implicit supersaturation constraint (because absorption by liquid water is much stronger than by vapor) and correlation between humidity and liquid water. The logarithm creates error characteristics that are more closely Gaussian and prevents unphysical retrieval of negative humidity.

The background error covariance $\mathbf{B}$ describes the expected variance at each level between the forecast and true state vector and the correlations between them. In this paper, $\mathbf{B}$ was taken from that used to assimilate data from satellite instruments operationally at the Met Office. The diagonal components of $\mathbf{B}$ are shown later for reference in Fig. 3.

III. OBSERVATIONS

This paper synthesizes observations from the Radiometrics TP/WVP-3000 microwave radiometer [6], which has 12 channels: Seven in the oxygen band 51–59 GHz, to provide information primarily on the temperature profile, and five between 22–30 GHz near a water vapor line, to provide humidity and cloud information. (However, frequencies below $\sim$53 GHz are also sensitive to moisture.) This radiometer includes sensors to measure pressure, temperature, and humidity at $\sim$1 m above the surface. The instrument's integral rain sensor is used to reject periods that may be contaminated by scattering from precipitation, as this is not included in the forward model, and emission from raindrops on the radome, which may bias the calibration. This instrument incorporates an optional zenith-viewing infrared radiometer (9.6–11.5 μm) to provide information on the cloud base temperature.

In this paper, the observation vector $\mathbf{y}$ is defined as a vector of the zenith brightness temperatures T_b that is measured by the radiometer's 12 channels, with additional elements for the surface temperature T_{AMB} and humidity (converted to $\ln q_{AMB}$) and the infrared brightness temperature T_{ir}, i.e.,

$$\mathbf{y} = [T_{b1}, T_{b2}, \ldots, T_{b12}, T_{AMB}, \ln q_{AMB}, T_{ir}]. \quad (2)$$

The observation error covariance $\mathbf{R}$ has contributions from the radiometric noise ($\mathbf{E}$), forward model ($\mathbf{F}$), and representativeness ($\mathbf{M}$) errors ($\mathbf{R} = \mathbf{E} + \mathbf{F} + \mathbf{M}$). The magnitude of each term of $\mathbf{R}$ is shown as $\sqrt{\mathrm{diag}(\mathbf{R})}$ in Table I for the 12 channels of the microwave radiometer, surface temperature, and humidity sensors (as dimensionless $\ln q$) and infrared radiometer.

The radiometric noise $\mathbf{E}$ can be evaluated as the covariance of $\mathbf{y}$ measured while viewing a stable scene (such as a liquid nitrogen target) over a short period ($\sim$30 min). $\mathbf{E}$ is approximately diagonal—i.e., the channels are independent—with

TABLE I
DIAGONAL COMPONENTS OF OBSERVATIONS' ERROR COVARIANCE
MATRIX $\sqrt{\mathrm{diag}(\mathbf{R})}$ EVALUATED FOR ALL DRY WEATHER CONDITIONS

Channel	Measurement Noise, $\mathbf{E}$	Modeling Errors, $\mathbf{F}$	Representativeness Error, $\mathbf{M}$	Total Uncertainty, $\mathbf{R}$	Units
22.235 GHz	0.17	0.83	0.65	1.07	K
23.035 GHz	0.12	0.84	0.67	1.08	K
23.835 GHz	0.11	0.82	0.69	1.08	K
26.235 GHz	0.13	0.67	0.78	1.04	K
30.000 GHz	0.21	0.61	1.00	1.19	K
51.250 GHz	0.18	1.10	1.70	2.04	K
52.280 GHz	0.15	0.88	1.35	1.62	K
53.850 GHz	0.17	0.35	0.32	0.50	K
54.940 GHz	0.18	0.06	0.10	0.14	K
56.660 GHz	0.19	0.05	0.10	0.22	K
57.290 GHz	0.54	0.05	0.40	0.67	K
58.800 GHz	0.18	0.06	0.11	0.22	K
T_{AMB}	0.17	0.00	0.22	0.28	K
$\ln q_{AMB}$	0.01	0.00	0.02	0.02	
T_{ir}	0.78	0.27	9.10	9.14	K

diagonal terms $\sim(0.1$–0.2 K$)^2$, except the 57.29-GHz channel of this particular instrument, as shown in Table I.

The forward model error $\mathbf{F}$ includes contributions from uncertainties in the spectroscopy and errors introduced by the profile discretization and model approximations (see Section IV). The spectroscopic component was estimated as the covariance of the difference in zenith T_b, which was calculated using two absorption codes [7], [8]. The other terms were calculated as the covariance of the difference between T_b, which was calculated using the full line-by-line model at high vertical resolution and the approximations. $\mathbf{F}$ contains significant off-diagonal terms and is the largest for the channels that are most sensitive to the water vapor continuum (26–52 GHz), where it reaches $\sim(1.1$ K$)^2$.

The representativeness error $\mathbf{M}$ allows for the radiometer's sensitivity to fluctuations on smaller scales than those represented by the NWP model. It is possible to estimate $\mathbf{M}$ by studying the fluctuations in the radiometer's signal on typical timescales taken for atmospheric changes to advect across the horizontal resolution of the NWP model. In the case of the mesoscale model with a 12-km grid, 1200 s was chosen to represent a typical advection timescale. The root-mean-square (rms) difference (divided by $\sqrt{2}$) in $\mathbf{y}$ that was measured over this time interval was used to calculate $\mathbf{M}$, after subtracting the contribution from the radiometric noise $\mathbf{E}$. This showed strong correlation between those channels that are sensitive to liquid water, water vapor, and temperature, respectively. However, this method is likely to underestimate the spatial variability for the surface sensors, which are strongly coupled to surface properties. The moisture terms were found to vary by an order of magnitude, depending on the atmospheric conditions. The average values of $\mathbf{M}$ that were calculated over a seven-day
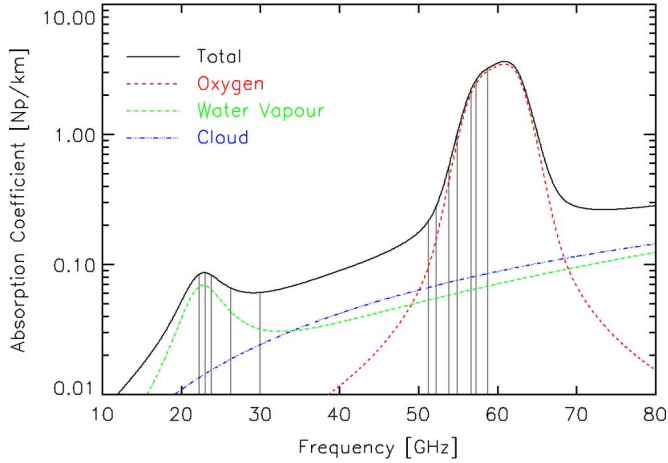
Fig. 1. Atmospheric absorption spectrum for typical surface conditions: $T = 288.15$ K, $p = 1013.25$ hPa, $RH = 100\%$, and $L = 0.2$ g/m^3 following [5]. Line styles show total absorption coefficient and contribution from oxygen, water vapor, and cloud liquid (L) according to the legend. Vertical bars indicate the center frequencies of the Radiometrics TP/WVP-3000 microwave radiometer.
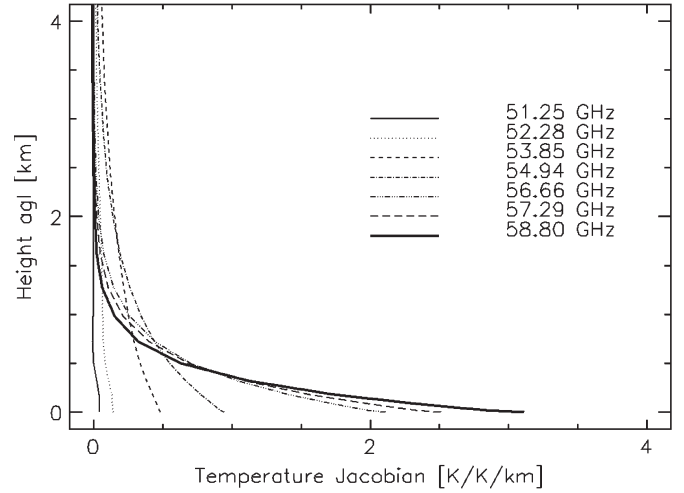

Fig. 2. Jacobian's temperature components for the 51–59-GHz channels of Radiometrics TP/WVP-3000, scaled by model layer thickness Δz: $\mathbf{H}/\Delta z$.

period of dry conditions with variable cloud amounts were taken to be typical. This period was later subdivided into clear and cloudy samples based on T_{ir} (see Section VIII), and $\mathbf{M}$ was reevaluated for each. The representativeness term that was evaluated in this way dominates the observation error covariance of some channels, with terms $\sim(0.1\text{–}1.7 \text{ K})^2$. $\mathbf{M}$ would be proportionally smaller for high-resolution models. $\mathbf{M}$ can also be evaluated dynamically, based on time series of observations within 1-h window of each observation. This technique allows the errors to be reduced in periods of atmospheric stability, when more confidence can be placed that the radiometer observations are representative of the model's state.

IV. FORWARD MODEL AND ITS JACOBIAN

A forward model $H(\mathbf{x})$ is needed to transform from state space to observation space. For the microwave radiometer, each channel's T_b is calculated at an equivalent monochromatic frequency [9] using the radiative transfer equation to integrate downwelling emissions from each atmospheric layer between model levels using a standard absorption model [7], which was found to have small biases in these channels [10]. The forward model for the surface temperature and humidity sensors is trivial—a $1:1$ translation to the lowest level of the state vector $\mathbf{x}$. A simple forward model defines T_{ir} as the temperature of the lowest level with any cloud. A more sophisticated radiative transfer model is used here to calculate T_{ir}, which accounts for extinction by atmospheric water vapor and liquid water cloud, assigning extinction coefficients of 0.02 Np/km $\cdot$ (kg/kg)$^{-1}$ and 33.3 Np/km $\cdot$ (kg/m^3)$^{-1}$, respectively [5]. This model gives more Gaussian error characteristics, due to having less abrupt transitions at cloud boundaries. Examples of the forward model and its Jacobian are shown in Figs. 1 and 2.

The *Jacobian* is the matrix of the sensitivity of the observation vector $\mathbf{y}$ to perturbations of each element of the state vector $\mathbf{x}$, i.e., $\mathbf{H} = H'(\mathbf{x}) = \nabla_{\mathbf{x}}\mathbf{y}$. It is needed to minimize the cost function (see Section VI). In this paper, $\mathbf{H}$ is calculated

by *brute force*—each level of the state vector $\mathbf{x}$ is perturbed by 1 K in temperature or 0.001 in $\ln q_t$. The magnitudes of these perturbations were selected to ensure linearity of $\mathbf{H}$ while preventing numerical errors due to truncation.

However, to speed up the calculation, a *fast absorption predictor* model is used to calculate the absorption in each level below 100 hPa as a third-order polynomial function of pressure, temperature, and q following [1]. This introduces an additional error in the calculation of T_b, as aforementioned. $\mathbf{H}$ is only calculated for levels between 0 and 8 km above ground level, corresponding to the maximum range of likely impact from the radiometer data, as can be seen in Fig. 2. For levels above this, $\mathbf{H} = 0$.

V. ERROR ANALYSIS

An estimate of the uncertainty in the retrieved profile can be derived by assuming that the errors are normally distributed about the solution and that the problem is only moderately nonlinear. In this case, the error covariance matrix of the analysis, i.e., $\mathbf{A}$, is given [2] by

$$\mathbf{A} = \left(\mathbf{H}_i^T \mathbf{R}^{-1} \mathbf{H}_i + \mathbf{B}^{-1}\right)^{-1} \qquad (3)$$

where $\mathbf{H}_i$ is evaluated at the solution (or final iteration).

It is also possible to express the information content of the observations with respect to the background as the degrees of freedom for signal (DFS), which represents the number of layers in the retrieved profile that are retrieved independently [2], i.e.,

$$\text{DFS} = \text{Tr}(\mathbf{I} - \mathbf{A}\mathbf{B}^{-1}) \qquad (4)$$

where $\mathbf{I}$ is the identity matrix, and $\text{Tr}(\cdot)$ is the trace operator.

$\mathbf{A}$ has been evaluated for different combinations of instruments for a *clear* U.S. standard atmosphere in Fig. 3, although it depends on the reference state through $\mathbf{H}_i$. This shows that the error in the temperature profile that is retrieved from the radiometer is expected to approach 0.1 K near the surface, but it increases with height, to exceed 1 K above 5 km, and includes
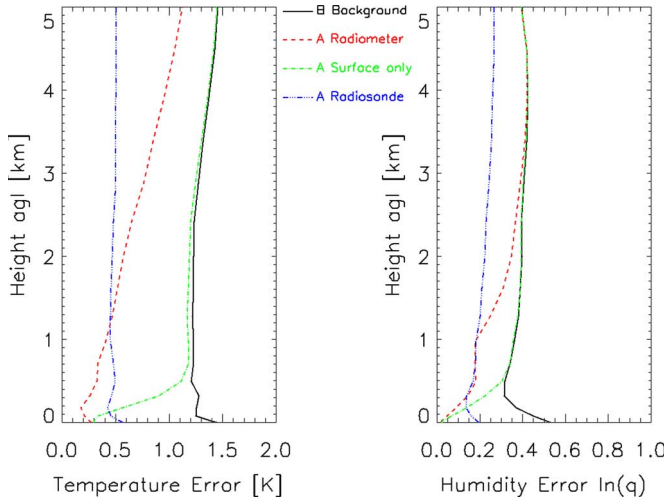
Fig. 3. (Solid) Background error covariance from mesoscale model $\sqrt{\text{diag}}(\mathbf{B})$ and analysis error covariances $\sqrt{\text{diag}}(\mathbf{A})$ with (dash-dot) surface sensors only, (dashes) radiometers and surface sensors, and (dash-dot-dot) radiosonde only. Plotted as square root of the matrices' diagonal components for the lowest 5 km of temperature (in kelvins) and humidity ($\ln q$) (dimensionless).

2.8 DFS. For the humidity profile, $\mathbf{A}$ varies greatly with $\mathbf{x}$. In this example, the retrieval's $\ln q$ error increases from 0.05 ($\sim$5%) near the surface to 0.4 ($\sim$40%) by 3 km and includes 1.8 DFS. DFS increases by $\sim$1.0 in cloudy conditions due to the extra information that is available from T_{ir}. These results show a substantial improvement on the background and the surface sensors alone, which only influence the lowest 500 m.

The performance of the retrievals from radiometer data can be compared to radiosondes. $\mathbf{A}$ was recalculated using errors currently assumed in the operational assimilation of radiosonde data at the Met Office, which are diagonal and dominated by representativeness. Fig. 3 shows that radiosondes provide more accurate analysis above 1 km than the radiometer for both temperature and humidity. However, below 1 km, the radiometer retrievals are comparable to radiosondes and provide much more frequent observations than radiosondes can, reducing errors of representativeness by applying their data to analysis at arbitrary times.

However, $\mathbf{A}$ only tells part of the story. The other important aspect of the retrieval's performance is the vertical resolution—its ability to resolve a perturbation in state space. One simple robust definition of the vertical resolution is the inverse of the diagonal of the *averaging kernel matrix* [2], which is scaled by the layer spacing. This is evaluated in Fig. 4, which shows that the vertical resolution of temperature profiles degrades with height, from $\sim$700 m near the surface, approximately linearly as twice the height from 0.5 to 4 km. For $\ln q$, it degrades very rapidly above 1.6 km, from $\sim$1.6 km near the surface, but is critically dependent on the reference state $\mathbf{x}$ due to nonlinearity in $\mathbf{H}$. Fig. 4 shows that the temperature information is concentrated in the lowest few kilometers but drops off steadily with height, whereas for humidity, it is all concentrated in the lowest 2 km in this example.

The apparent degradation of vertical resolution near the surface is due to the assumed correlations in $\mathbf{B}$. If the correlations between the six lowest levels in $\mathbf{B}$ are suppressed by a factor
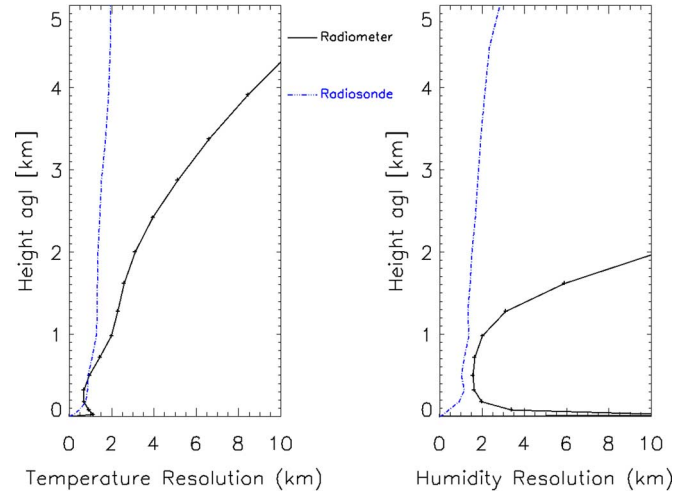

Fig. 4. Vertical resolution of temperature and humidity ($\ln q$) for radiosonde and 1D-VAR radiometer retrievals in clear U.S. standard atmosphere found using the aforementioned averaging kernel matrix method, which depends on the case that is considered, due to nonlinearity in $\mathbf{H}$.

of 10 for both temperature and humidity, the resulting vertical resolutions do not increase near the surface in this way. This sensitivity to the choice of $\mathbf{B}$ makes it difficult to compare these results with other definitions, which tend to produce more optimistic results [11], [12].

VI. MINIMIZATION OF COST FUNCTION

Variational retrievals are performed by selecting the state vector that minimizes a cost function in the form of (1). For linear problems, where $\mathbf{H}$ is independent of $\mathbf{x}$, this can be solved analytically. However, the retrieval of temperature profiles above $\sim$1 km and humidity profiles is moderately nonlinear; thus, the minimization must be conducted numerically. This has been achieved using the Levenberg–Marquardt method [2] (which was found to improve the convergence rate in cloudy conditions as compared to the Gauss–Newton method) by applying the following analysis increments iteratively:

$$\mathbf{x}_{i+1} = \mathbf{x}_i + \left((1+\gamma)\mathbf{B}^{-1} + \mathbf{H}_i^T \mathbf{R}^{-1} \mathbf{H}_i \right)^{-1}$$
$$\cdot \left[\mathbf{H}_i^T \mathbf{R}^{-1} \left(\mathbf{y} - H(\mathbf{x}_i) \right) - \mathbf{B}^{-1} (\mathbf{x}_i - \mathbf{x}^{\mathbf{b}}) \right] \quad (5)$$

where $\mathbf{x}_i$ and $\mathbf{x}_{i+1}$ are the state vectors before and after iteration i, respectively, $\mathbf{H}_i$ is the Jacobian matrix at iteration i, and γ is a factor that is adjusted after each iteration depending on how $J(\mathbf{x})$ has changed. As $\gamma \to 0$, the step tends toward the same as the Gauss–Newton method; as $\gamma \to \infty$, it tends to the steepest decent of $J(\mathbf{x})$.

Equation (5) is iterated until the following convergence criterion [2] is satisfied, based on a χ^2 test of the residuals of $[\mathbf{y} - H(\mathbf{x})]$:

$$\left[(H(\mathbf{x}_{i+1}) - H(\mathbf{x}_i)) \right]^T \mathbf{S}_{\delta\mathbf{y}}^{-1} \left[(H(\mathbf{x}_{i+1}) - H(\mathbf{x}_i)) \right] \ll m \quad (6)$$

where $\mathbf{S}_{\delta\mathbf{y}}$ is the covariance matrix between $\mathbf{y}$ and $H(\mathbf{x}_i)$, and m is the dimension of $\mathbf{y}$ ($m = 15$ in this case).
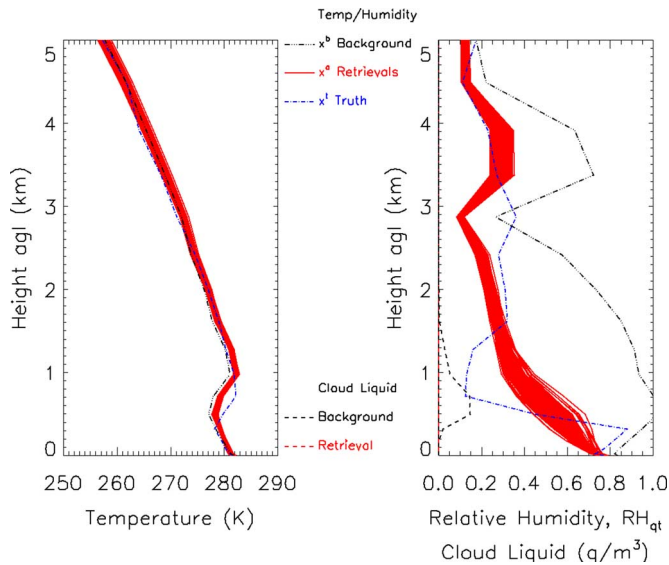
Fig. 5. Example retrievals with 105 synthetic observations, with profiles between NWP model background and truth. Left panel shows temperature profiles. Right panel shows profiles of relative humidity ($RH_{qt} = q_t/q_{sat}$) and (dotted line) cloud liquid water content (in grams per cubic meter).
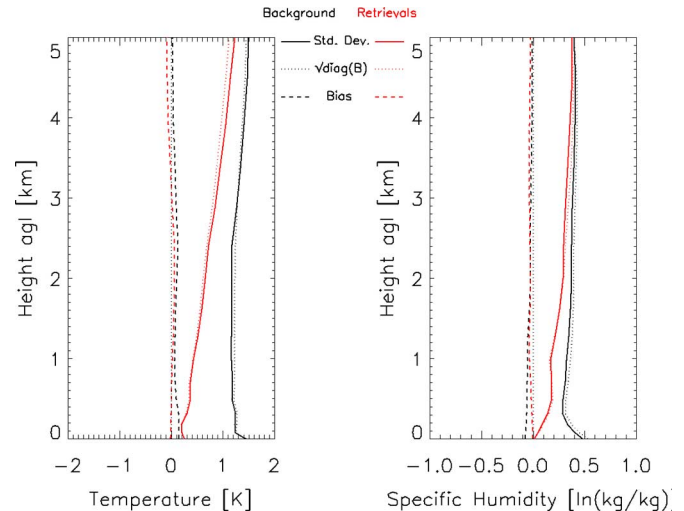

Fig. 6. Statistics of 1D-VAR retrievals using synthetic observations and background for 314 cases from Camborne. Solid lines show standard deviation of difference between retrieved and sonde profiles. Dashed lines show bias. Theoretical error covariances are shown as dotted lines for the analysis, $\sqrt{\mathrm{diag}(\mathbf{A})}$, and the background, $\sqrt{\mathrm{diag}(\mathbf{B})}$. Red lines show statistics of all the 1D-VAR retrievals, whereas black lines show statistics of the background.

Convergence typically takes three to ten iterations, each requiring ~ 0.25 s of central processing unit time on a 2.4-GHz Pentium IV using the *fast absorption predictor* model.

Upon convergence, the retrieved state vector $\hat{\mathbf{x}}$ is tested for statistical consistency with $\mathbf{y}$ and $\mathbf{R}$ by calculating the value of

$$\chi^2 = [H(\hat{\mathbf{x}}) - \mathbf{y}]^T \mathbf{R}^{-1} [H(\hat{\mathbf{x}}) - \mathbf{y}]. \qquad (7)$$

Retrievals with a $\chi^2 > 100$ were rejected. The choice of χ^2 threshold was found not to be critical, as it had a small influence on the statistics of the retrievals.

VII. EXAMPLE OF 1D-VAR RETRIEVALS

Fig. 5 shows an example of the 1D-VAR retrievals using synthetic observations, which are generated to be consistent with $\mathbf{R}$. These are based on a real radiosonde profile for Camborne, U.K., at 11:21 on December 9, 2004, and NWP background profile from a 5-h forecast, valid 21 min earlier. This case was selected because the model had forecast the inversion ~ 200 m too low and overestimated the humidity by a factor of ~ 2 over the whole profile. The retrieval was repeated for 100 such sets of observations, all of which converged in four iterations. The retrieved profiles are closely clustered with typical standard deviations of 0.2–0.5 K in temperature and 0.05–0.10 in $\ln q$, showing that they are relatively robust in the presence of observation noise. In this example, all retrievals thin the cloud and give profiles closer to the truth than the background. However, the correlation between temperature at adjacent levels of $\mathbf{B}$ makes it impossible for the retrieval to move a misplaced feature in the vertical without additional information—e.g., observations at lower elevation angles.

VIII. CLOUD CLASSIFICATION SCHEME

Examination of the performance of the retrieval scheme showed that there were often problems when the humidity approaches the threshold of cloud formation—the residuals often oscillate without reaching convergence. This was partially improved by the implementation of the Levenberg–Marquardt method of minimization, which adjusts the size of the increment at each iteration to change from the classic Gauss–Newton method toward the method of steepest decent, based on whether the previous iteration has reduced J.

Convergence problems where $\ln q_t$ approaches the cloud threshold can also be caused by the error characteristics of T_{ir}, which can be highly non-Gaussian. This has been addressed by introducing a cloud classification as a preprocessing step to the retrieval, which is based on a threshold of the infrared brightness temperature T_{ir}. If the observed (or synthetic) $T_{\mathrm{ir}} > \max\{T_{\mathrm{AMB}} - 40 \text{ K}, 223 \text{ K}\}$, the profile is classified as *cloudy*, and the retrieval proceeds as described previously in the text. Otherwise, the profile is classified as *clear*, and the control variable changed from $\ln q_t$ to the log of the specific humidity $\ln q$, and an additional term [13] is added to the cost function to prevent saturation. In *clear* cases, the representativeness term can be reduced by reevaluating it in only clear sky conditions to allow more accurate retrievals in clear conditions.

IX. STATISTICS OF 1D-VAR RETRIEVALS

1D-VAR retrievals were performed on an extended data set of one year of radiosonde profiles from Camborne but using synthetically generated observations and backgrounds, which were consistent with $\mathbf{R}$ and $\mathbf{B}$, respectively. Cloud was generated at levels where $RH > 90\%$ by converting the radiosondes' humidity to total water. The statistics for the combined *clear* and *cloudy* cases, as shown in Fig. 6, are in good agreement

with the expected performance from the error analysis, with a convergence rate of 75%. There is no significant difference in the performance in clear and cloudy cases, although the convergence rate is poorer in cloudy conditions. The background profiles have a small bias, which is corrected in the retrievals.

The application of this method to real observations and background from NWP models introduces biases and non-Gaussian error characteristics, which slightly reduces the convergence rate. If they are sufficiently stable, biases may be reduced by correcting the observations with respect to the background prior to performing the retrieval.

The retrieved values of integrated water vapor (IWV) were also compared to the radiosonde values. These were found to be good, with a small bias and a standard deviation of 0.88 kg/m^2, providing a substantial improvement on the corresponding value for the synthetic backgrounds (2.00 kg/m^2), and compared favorably with other methods, which have been shown to retrieve IWV from microwave radiometer observations with an accuracy of better than 1.0 kg/m^2 as compared to radiosondes in midlatitude winter [14]. This implies that the retrievals do not need an additional constraint in the cost function to force the IWV to match that retrieved by a simpler method, as this is achieved implicitly in the 1D-VAR retrievals.

X. CONCLUSION AND FUTURE WORK

A 1D-VAR retrieval has been developed to allow observations from ground-based microwave and infrared radiometers and surface sensors to be combined with a background from an NWP model in an optimal way, which accounts for their error characteristics. This has been shown to be advantageous over methods taking their background from statistical climatology [15]. The 1D-VAR method has been used to retrieve profiles of temperature, humidity, and clouds using a novel total water control variable.

The observation errors for channels that were sensitive to clouds were dominated by representativeness errors. To reduce their impact, these can be evaluated dynamically. Convergence problems were encountered in cloudy cases, partially due to the non-Gaussian error characteristics of the infrared observations. A cloud classification scheme has been introduced to address this and help constrain the retrievals.

The 1D-VAR retrievals also have the advantage of providing an estimate of the error in the retrieved profile. Error analysis has shown that the microwave radiometer improves the NWP background up to 4 km, retrieving temperature profiles with < 1 K uncertainty and 2.8 DFS and humidity with $< 40\%$ uncertainty and 1.8 degrees of freedom. These results depend on the background error covariance. However, the vertical resolution of the retrieved profiles is poor and degrades with height. Furthermore, the retrievals were not able to move a misplaced feature in the background temperature profile.

The variational method allows different instruments to be combined if their observations' forward model operator and error estimates are available. This provides a basis for the development of *integrated profiling systems*. In the future, the 1D-VAR retrievals will be extended to include observations from other instruments, such as the cloud base height from a ceilometer, cloud base/top from cloud radar, and refractive index gradient from a wind profiler.

Assimilation of these observations could improve mesoscale NWP, particularly boundary layer and cloud properties. However, fully exploiting the high time resolution that is available from ground-based instruments will require 4-D variational assimilation.

REFERENCES

[1] U. Löhnert, S. Crewell, and C. Simmer, "An integrated approach toward retrieving physically consistent profiles of temperature, humidity, and cloud liquid water," *J. Appl. Meteorol.*, vol. 43, no. 9, pp. 1295–1307, Sep. 2004.

[2] C. D. Rodgers, *Inverse Methods for Atmospheric Sounding: Theory and Practice*. Singapore: World Scientific, 2000.

[3] K. Ide, P. Courtier, M. Ghil, and A. C. Lorenc, "Unified notation for data assimilation: Operational, sequential, and variational," *J. Meteorol. Soc. Jpn.*, vol. 75, no. 1B, pp. 181–189, 1997.

[4] G. Deblonde and S. J. English, "One-dimensional variational retrievals from SSMIS simulated observations," *J. Appl. Meteorol.*, vol. 42, no. 10, pp. 1406–1420, Oct. 2003.

[5] T. J. Hewison, "Profiling temperature and humidity by ground-based microwave radiometers," Ph.D. thesis, Univ. Reading, Reading, U.K., 2006.

[6] R. Ware, F. Solheim, R. Carpenter, J. Gueldner, J. Liljegren, T. Nehrkorn, and F. Vandenberghe, "A multi-channel radiometric profiler of temperature, humidity and cloud liquid," *Radio Sci.*, vol. 38, no. 4, pp. 8079–8092, 2003.

[7] P. W. Rosenkranz, "Water vapor microwave continuum absorption: A comparison of measurements and models," *Radio Sci.*, vol. 33, no. 4, pp. 919–928, 1998. Subsequent correction in *Radio Sci.*, vol. 34, no. 4, p.1025, 1999.

[8] H. J. Liebe, G. A. Hufford, and M. G. Cotton, "Propagation modeling of moist air and suspended water/ice particles at frequencies below 1000 GHz," presented at the AGARD 52nd Specialists' Meeting Electromagnetic Wave Propagation Panel, Palma de Mallorca, Spain, May 17–21, 1993, Paper 3/1-10.

[9] D. Cimini, T. J. Hewison, and L. Martin, "Comparison of brightness temperatures observed from ground-based microwave radiometers during TUC," *Meteorol. Z.*, vol. 15, no. 1, pp. 19–25, Feb. 2006.

[10] T. J. Hewison, D. Cimini, L. Martin, C. Gaffard, and J. Nash, "Validating clear air absorption model using ground-based microwave radiometers and vice-versa," *Meteorol. Z.*, vol. 15, no. 1, pp. 27–36, Feb. 2006.

[11] T. M. Scheve and C. T. Swift, "Profiling atmospheric water vapor with a K-band spectral radiometer," *IEEE Trans. Geosci. Remote Sens.*, vol. 37, no. 3, pp. 1719–1729, May 1999.

[12] J. C. Liljegren, S. A. Boukabara, K. Cady-Pereira, and S. A. Clough, "The effect of the half-width of the 22-GHz water vapor line on retrievals of temperature and water vapor profiles with a 12-channel microwave radiometer," *IEEE Trans. Geosci. Remote Sens.*, vol. 43, no. 5, pp. 1102–1108, May 2005.

[13] L. Phalippou, "Variational retrieval of humidity profile, wind speed and cloud liquid-water path with SSM/I: Potential for numerical weather prediction," *Q. J. R. Meteorol. Soc.*, vol. 122, no. 530, pp. 327–355, Jan. 1996.

[14] L. Martin, C. Mätzler, T. J. Hewison, and D. Ruffieux, "Intercomparison of integrated water vapour measurements," *Meteorol. Z.*, vol. 15, no. 1, pp. 57–64, Feb. 2006.

[15] D. Cimini, T. J. Hewison, L. Martin, J. Güldner, C. Gaffard, and F. S. Marzano, "Temperature and humidity profile retrievals from ground-based microwave radiometers during TUC," *Meteorol. Z.*, vol. 15, no. 5, pp. 45–56, 2006.

Tim J. Hewison (M'96) received the Ph.D. degree in meteorology from the University of Reading, Reading, U.K. This work was taken from his thesis on the use of ground-based microwave radiometers.

He is currently with the Met Office, University of Reading, where he is working toward the integration of their data with other instruments and their assimilation into NWP to redesign the upper-air observing network.